*31st EPS Conference on Plasma Phys. London, 28 June - 2 July 2004 ECA Vol.**28G**, P-4.191 (2004)*

H-modes in single null diverted configuration on MAST

H. Meyer, S. Saarelma, A. Kirk, P.G. Carolan, G.F. Counsell, G. Cunningham, M.J. Walsh[†], H.R. Wilson and the MAST and NBI Teams

EURATOM/UKAEA Fusion Association, Culham Science Centre, Abingdon, Oxfordshire, OX14 3DB, UK

[†]*Walsh Scientific Ltd., Culham Science Centre, Abingdon, Oxfordshire, OX14 3EB, UK*

Introduction

Large spherical tokamaks (STs) such as MAST and NSTX operate routinely in ELMy H-mode [1, 2], the baseline scenario for the next step fusion device ITER. The performance of ITER is extrapolated from existing results on the basis of empirical scaling laws. The different geometry and parameter space of an ST helps to resolve ambiguities in these scaling laws hence making them more reliable. Furthermore, the different conditions in an ST may also improve the understanding of the physics of transport barrier formation and pedestal stability.

On MAST most H-modes are observed in a magnetic topology where two poloidal field nulls, X-points, are on the last closed flux surface (LCFS). Such a connected double null (C-DN) configuration allows H-mode access at auxiliary heating levels reduced by more than a factor of 2 compared to similar disconnected double null (D-DN) or single null (SN) configurations with the ion ∇B-drift directed towards the X-point on the LCFS [3]. Conventional tokamaks, on the other hand, usually operate in SN, although recently operation close to DN has gained interest with respect to access to the favourable type-II ELMy regime [4].

To enable better comparison of MAST H-modes with conventional tokamaks lower SN (L-SN) configurations have been studied with respect to H-mode physics, scrape-off-layer (SOL) behaviour and confinement. Operation in L-SN is achieved on MAST with unbalanced currents in the upper and lower divertor coils. In this paper we compare the H-mode characteristics between C-DN and L-SN and present initial investigations of the ideal MHD stability of the plasma edge.

Characteristics of L-SN H-modes

Two L-SN configurations with different upper triangularity $\delta_u = 0.25$ and $\delta_u = 0.32$ have been developed on MAST. The lower triangularity $\delta_l = 0.46$ determined by the X-point is similar in both configurations. H-mode in L-SN could so far only be accessed in the configuration with the lower triangularity. The maximum plasma current in L-SN is $I_p < 0.7$ MA at present, because of limitations of the power supplies of the divertor coils. Using a specific start-up method with low initial current from merging compression $I_p^{MC} < 100$ kA followed by a relatively fast current ramp $dI_p/dt \geq 3$ MA/s (Scenario 1) the appearance of the $q = 1$ surface in the plasma can be delayed. In this scenario, depending on the amount of neutral beam power, P_{NBI}, and dI_p/dt the first sawtooth crash is usually later than $t = 260$ ms. With $I_p^{MC} \geq 400$ kA (Scenario 2) the first sawtooth can occur as early as $t \approx 100$ ms. In all L-SN discharges the current is evolving throughout the discharge. In Scenario 2 the L/H transition is triggered by the first sawtooth crash with $P_{NBI} \geq 1$ MW. In Scenario 1 on the other hand the L/H transition occurs early well before the first sawtooth and sometimes even during the current ramp-up. Here, only $P_{NBI} > 0.35$ MW is needed to achieve a clear L/H transition 50 ms after beam heating is switched on. Even with Ohmic heating alone marginal H-mode can be achieved transiently in L-SN.

In Fig. 1 the plasma current (a), Greenwald fraction n_G (b), H_H factor (c), normalised β (d), D_α emission (e), and the injected neutral beam power (f) are shown for comparable L-SN (black) and C-DN (red, green) discharges. The L/H transitions are marked for each discharge by the vertical blue lines in the graph (e). The most striking difference between L-SN and C-DN discharges on MAST is the absence of clear ELMs in L-SN. Note, the periodic D_α spikes in discharge #9447 between 0.09 s $< t <$ 0.155 s (see Fig. 1e, black) are not

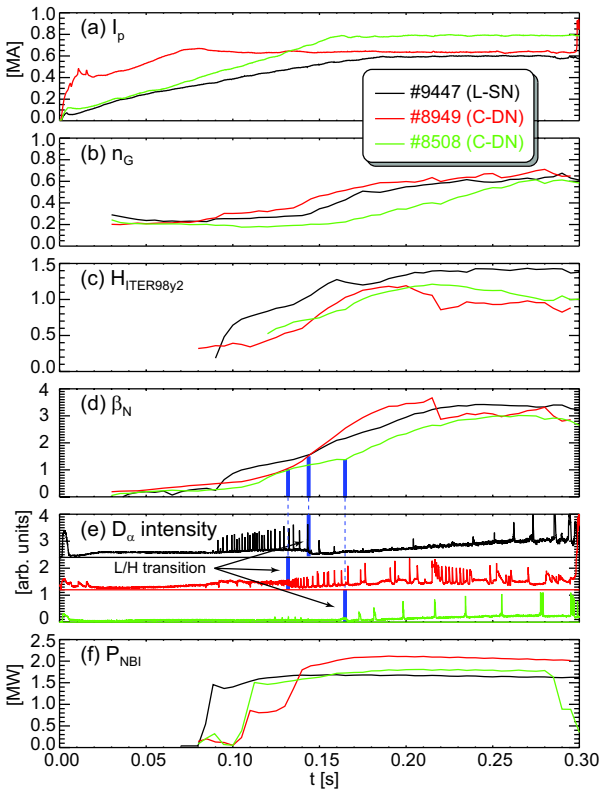

Figure 1: *Comparison of L-SN (black) and C-DN (red,green) H-mode discharges.*

ELMs. They start before the L/H transition and are associated with magnetic activity around 100 kHz probably due to the high beam power and low density. ELMs on MAST at input powers up-to $P_{\rm NBI} < 2.5$ MW show typically the characteristics of type-III ELMs [5]. As can be seen from Fig. 1e, both the C-DN discharges show ELMs whereas the L-SN discharge (#9447, black) has a long ELM-free period at similar (#8949,green) or higher (#8508, red) Greenwald fraction (Fig. 1b). Consequently the confinement with $H_{\rm H} = \tau_{\rm E}/\tau_{\rm ITER98y2} = 1.4$ is best in the L-SN discharge (Fig. 1c). Later in discharge #9447 ($t > 0.26$ s) sawtooth crashes are followed by short D_α bursts, which might be ELMs. A reduction of $P_{\rm NBI}$ should destabilise ELMs on MAST, because of the type-III nature. However, in a series of discharges similar to #9447, where $P_{\rm NBI}$ was reduced until sustained H-mode was lost (purely Ohmic heating) no ELMs were found.

Interestingly, the slope of $\bar{n}_{\rm e}$ drops at $t = 0.172$ ms without degradation of confinement, although fuelling is sustained. Fluctuations of the D_α emission increase at $t = 0.158$ ms accompanied by "chirping" bursts of magnetic activity around 35 kHz.

This can be seen from Fig. 2 which shows a wavelet transform of the signal of an LFS Mirnov coil measuring the vertical field fluctuations. The discharge conditions at $t = 0.158$ ms are: $I_{\rm p} = 540$ kA, $n_{\rm G} = 0.4$, $q_{95} = 9$, $\delta = 0.37$, $\kappa = 1.8$, $\beta_{\rm p} = 0.56$, and $\beta_{\rm N} = 2.1$. The magnetic signature of the mode is consistent with that of an $n = 1$, $m \approx 2$ core mode. The mode can also be seen on the central soft X-ray chords. However, a correlation of the D_α fluctuations with the mode was found. Whether the enhanced D_α fluctuation level can be associated to type-II or other small ELMs is still an open question.

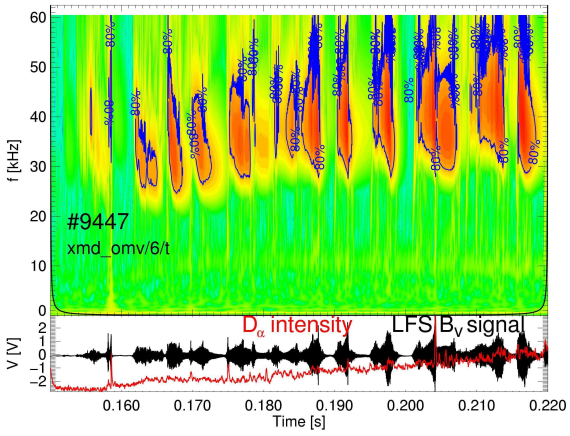

Figure 2: *Wavelet transform of B_v fluctuations at the LFS for discharge #9447.*

Typical Thomson scattering (TS) profiles of $n_{\rm e}$, $T_{\rm e}$ and $p_{\rm e}$ for H-mode in L-SN are shown in Fig. 3 for two shots with similar $P_{\rm NBI} = 1.2$ MW but different refuelling. In shot #7508 (left) the refuelling was from both the high field side (HFS) and low field side (LFS), whereas shot #7572 (right) had only LFS fuelling until 40ms before the TS measurement ($t_{\rm TS} = 0.18$ ms). The density pedestal, $n_{\rm e}^{\rm ped}$, in #7508 is 1.6 times higher than in #7572. However, the temperature pedestals, $T_{\rm e}^{\rm ped} \approx 130$ eV, are similar in both discharges comparing well to values observed in C-DN during long inter ELM periods. The LFS edge neutral density profiles are similar in both discharges. Neither the refuelling position nor the height of $n_{\rm e}^{\rm ped}$ affect $T_{\rm e}^{\rm ped}$ in SN on MAST indicating that it is predominantly

the heat transport across the transport barrier which determines T_e^{ped}.

The scrape-off-layer in MAST L-SN discharges behaves similarly to conventional tokamaks and narrows on the HFS and LFS by a factor of ~ 2 at the L/H transition. In C-DN a similar SOL narrowing and width is only observed on the LFS. The HFS SOL shows no significant narrowing at the L/H transition. The SOL width in L-mode at the LFS is comparable in L-SN and C-DN. At the HFS it is 4 times narrower in C-DN than in L-SN. The width of the SOL is roughly determined by the ratio between radial to parallel transport. In L-SN the HFS SOL is dominated by the parallel transport from the LFS and therefore by the radial transport at the LFS. In C-DN on the other hand there is no parallel connection between LFS and HFS and the HFS SOL width is determined by the lower radial transport at the HFS.

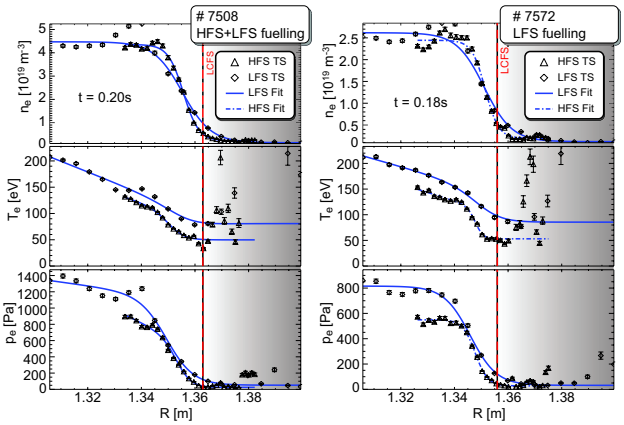

Figure 3: *HFS and LFS electron pedestal profiles for L-SN H-modes with different fuelling but the same* $P_{NBI} = 1.2$ MW.

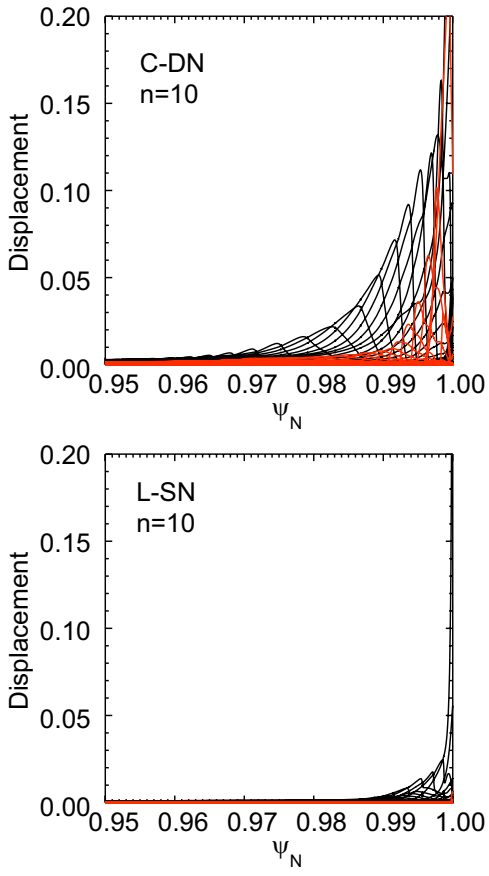

Figure 4: $n = 10$ *mode structure for C-DN (left) and L-SN (right) with the same kinetic edge profiles (black: real part, red: imaginary part).*

Peeling-ballooning stability

The influence of the proximity of a 2nd X-point on the ideal peeling-ballooning mode stability for medium ($n = 8$) to high toroidal mode numbers ($n = 24$) at the plasma edge was investigated using the ELITE code [6]. Peeling modes are edge kink instabilities resonant to rational surfaces just outside the plasma edge and are thought to play a key role in ELMs. They are stabilised by a pressure gradient and destabilised by the parallel current density. Ballooning modes on the other hand are driven unstable by an increasing pressure gradient, whereas an increase in parallel current density is stabilising by enabling access to second stability.

The stability calculations were based on the C-DN discharge #8901 ($I_p = 0.79$ MW, $B_t(R = 0.76\text{ m}) = 0.56$ T, $\bar{n}_e = 5.6 \times 10^{19}$ m^{-3}, $P_{NBI} = 2.4$ MW) and the L-SN discharge #7508 ($I_p = 0.52$ MW, $B_t(R = 0.76\text{ m}) = 0.53$ T, $\bar{n}_e = 3.6 \times 10^{19}$ m^{-3}, $P_{NBI} = 1.2$ MW) with profiles from the high resolution TS system assuming $T_i = T_e$. The kinetic profiles were taken 30 ms and 20 ms into a long ELM free period ($\Delta t \approx 40$ ms, $\Delta t \approx 25$ ms) for shot #8901 and #7508 respectively. Since the gradient at the LFS is underestimated for steep gradients, measurements from the HFS are used. In addition, an artificial L-SN discharge was created by changing the C-DN equilibrium to L-SN whilst retaining the kinetic profiles from the real C-DN discharge. This allows to study the effect of the magnetic configuration on the stability alone. The parallel current at the edge is dominated by the bootstrap current, j_{BS}, in H-mode. Here, the expression from Sauter et.al. is used [7, 8]. Note, that ELITE can't handle the separatrix but can approach diverted plasmas very closely. Similar investigations for lower mode numbers for ASDEX-Upgrade using the GATO code found DN

to be more stable than SN [9]. There, the radial extent of the modes was found to be much smaller in DN than in SN, consistent with the occurrence of type-II ELMs in these regimes.

Both, the C-DN and artificial L-SN equilibria (#8901) are unstable with profiles consistent with the measurements, whereas the real L-SN equilibrium (#7508) is stable. In Fig. 4 the mode structure for $n = 10$ is shown for C-DN (left) and the artificial L-SN (right) for an equilibrium with twice the experimental pedestal pressure, $p_{\rm ped} = 2p^{\rm exp.}_{\rm ped}$. In contrast to ASDEX-Upgrade, the radial extent is much larger in C-DN than in L-SN. For lower $p_{\rm ped}$, however, the structures in L-SN and C-DN become more similar and peeling like. The diamagnetic frequency, $\omega_\star$, exceeds the growth rate by about two orders of magnitude in a narrow region close to the edge. Therefore narrow peeling modes might be stabilised. The mode structure becomes much wider if the q-profile is flattened due to the high $j_{\rm BS}$. All discharges are stable with respect to the $n = \infty$ ballooning modes.

For all cases, scans in p' (see Fig. 5) were performed for $n = 8, 12, 16, 20, 24$. p' was changed by changing $T^{\rm ped}_{\rm e} = T^{\rm ped}_{\rm i}$ and keeping $n^{\rm ped}_{\rm e,i}$ constant, thus changing p' and $j_{\rm BS}$ simultaneously. In the experiment, however, it is $n^{\rm ped}_{\rm e}$ rather than $T^{\rm ped}_{\rm e}$ that increases during ELM free periods in H-mode, hence, p' increases but $j_{\rm BS}$ might decrease. The real L-SN configuration remains stable even if $p_{\rm ped} > 2p^{\rm exp.}_{\rm ped}$. The C-DN and the artificial L-SN configurations become stable only at $p_{\rm ped} < 0.5p^{\rm exp}_{\rm ped}$. Growth rates in L-SN are generally smaller than in C-DN, although for the C-DN/L-SN comparison with similar profiles this difference is small. Hence, it seems that the increased stability in L-SN is more related to the experimental profiles than to the proximity of the 2nd X-point.

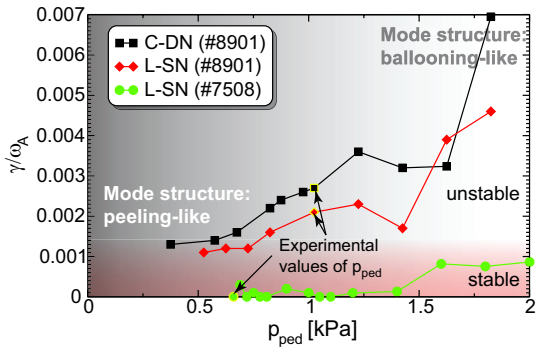

Figure 5: *Pressure gradient scan for C-DN (black), artificial L-SN (red) and L-SN (green).*

Conclusion

First H-modes in L-SN configuration were achieved on MAST with $H_{\rm H} = 1.4$. So far there is no clear indication of ELMs in L-SN. Pedestal temperatures and densities are comparable to C-DN discharges with long ELM free periods. The SOL in L-SN behaves similarly to conventional tokamaks and narrows by a factor of ~ 2 at the L/H transition.

Stability calculations using ELITE show that the L-SN discharges are ideal MHD stable at the edge and far away from the stability boundary. The C-DN discharge, on the other hand, is always unstable. An artificially created L-SN equilibrium with the same kinetic profiles as the C-DN case is also unstable with similar growth rates. Hence, the increased stability in L-SN originates from the difference in profiles between L-SN and C-DN.

Acknowledgements

This work was jointly funded by the UK Engineering and Physical Sciences Research Council and EURATOM.

References:

[1] AKERS, R. J. et al., Phys. Rev. Lett. **88** (2002) 035002.
[2] MAINGI, R. et al., Phys. Rev. Lett. **88** (2002) 35003.
[3] MEYER, H. et al., Plasma Phys. Control. Fusion **46** (2004) A291.
[4] STOBER, J. et al., Nucl. Fusion **41** (2001) 1123.
[5] KIRK, A. et al., Nucl. Fusion **46** (2003) 551.
[6] WILSON, H. R. et al., Phys. of Plasmas **9** (2002) 1277.
[7] SAUTER, O. et al., Phys. of Plasmas **6** (1999) 2834.
[8] SAUTER, O. et al., Phys. of Plasmas **9** (2002) 5140.
[9] SAARELMA, S. et al., Nucl. Fusion **43** (2003) 261.